Journal of Computational Physics 376 (2019) 924–936

Contents lists available at ScienceDirect

Journal of Computational Physics

www.elsevier.com/locate/jcp

A general framework for the evaluation of shock-capturing schemes

Guoyan Zhao [a], Mingbo Sun [a,*], Antonio Memmolo [b], Sergio Pirozzoli [b,*]

[a] Science and Technology on Scramjet Laboratory, National University of Defense Technology, Deya Road 109, Changsha 410073, China
[b] Dipartimento di Ingegneria Meccanica e Aerospaziale, Sapienza Università di Roma, Via Eudossiana 18, 00184 Roma, Italy

ARTICLE INFO

Article history:
Received 30 April 2018
Received in revised form 31 August 2018
Accepted 5 October 2018
Available online 9 October 2018

Keywords:
Shock capturing schemes
Computational efficiency
Wave propagation

ABSTRACT

We introduce a standardized procedure for benchmarking shock-capturing schemes which is intended to go beyond traditional case-by-case analysis, by setting objective metrics for cross-comparison of flow solvers. The main idea is that use of shock-capturing schemes yields both distributed errors associated with propagation of wave-like disturbances in smooth flow regions, and localized errors at shocks where nonlinear numerical mechanisms are most active. Our standardized error evaluation framework relies on previous methods of analysis for the propagation error with associated cost/error mapping, and on novel analysis of the shock-capturing error based on a model scalar problem. Amplitude and phase errors are identified for a number of classical shock-capturing schemes with different order of accuracy. Whereas all schemes are found to be, as expected, first-order accurate at shocks, quantitative differences are found to be significant, and we find that certain schemes in wide use (e.g. high-order WENO schemes) may yield substantial over-amplification of incoming disturbances at shocks. Illustrative calculations are also shown for the 1D Euler equations, which support sufficient generality of the analysis, although nonlinearity suggests caution in straightforward extrapolation to other flow cases.

1. Introduction

Computational fluid dynamics has undergone tremendous development as a discipline for several decades [1]. Complex structures as vortices, waves and shocks must be accurately resolved in the study of turbulent compressible flows. For that purpose, linear, central-difference approximations are ideal candidates as they yield minimal numerical diffusion and they are computationally efficient [2]. High-order central discretizations are in fact typically used in direct numerical simulation and large-eddy simulation of turbulent flows, as well as in computational aeroacoustics. However, it is known that for problems involving discontinuities like shocks or material interfaces, high-order central schemes inevitably introduce high-frequency oscillations whose amplitude does not decrease as the grid is refined (Gibbs phenomenon), which is usually unacceptable if accuracy is required [3].

Several alternatives are available to circumvent the failure of central schemes at shocks, most of which fall in the class of 'shock-capturing' schemes, whose main idea [4,5], is to activate (or enhance) numerical diffusion locally around discontinuities so as to prevent (or at least limit) the onset of Gibbs oscillations and stabilize computations. Many successful

* Corresponding authors.
E-mail addresses: sunmingbonudt@sina.cn (M. Sun), sergio.pirozzoli@uniroma1.it (S. Pirozzoli).

https://doi.org/10.1016/j.jcp.2018.10.013

shock-capturing algorithms have been proposed over the years, a few representative classes being: i) total variation diminishing (TVD) schemes [6], which rely on the use of flux or slope limiters to numerically enforce the condition of non-increase of the total variation in time, thus achieving oscillation-free solutions, however at the price of reduced order of accuracy at extrema; ii) essentially non-oscillatory (ENO) schemes [7], in which uniform high-order accuracy is achieved through the use of adaptive stencils to minimize the likelihood of crossing discontinuities; iii) weighted essentially non-oscillatory (WENO) schemes [8], which rely on convex combination of reconstructions carried out over many candidate stencils, with weights depending on the local smoothness of the solution on each stencil; iv) monotonicity-preserving (MP) schemes [9], which numerically enforce the condition of monotonicity preservation through the use of limiters, thus achieving uniformly high order of accuracy. Combinations of the above methods have also been sometimes used, for instance monotonicity-preserving WENO (MPWENO) schemes were developed by Balsara and Shu [10] to incorporate the MP property in classical WENO schemes. As previously noted, shock-capturing schemes are suboptimal for computing turbulent flows and for aeroacoustics applications, since inherent numerical diffusion causes damping of propagating waves. Hence, several efforts have been spent in recent years to alleviate these shortcomings. Some attempts fall in the class of hybrid methods [11,3], whereby shock sensors are used to locally apply shock-capturing schemes around shocks, or in the class of optimized methods, which are rather based on the attempt to modify the stencils, coefficients and/or weights of existing schemes, mainly WENO [12,13]. Ramifications of the shock-capturing idea are too disparate to be fully quoted here.

Evaluating the performance of shock-capturing schemes should account for several properties. First, their wave propagation properties in smooth flow regions should be addressed. Pirozzoli [14] quantified the leading-order effects of nonlinear mechanisms underlying shock-capturing schemes on the solution behavior in wavenumber space and introduced an empirical dispersion relation (EDR), which relies on numerical testing of individual sinusoidal waveforms with different wavenumbers. Although the EDR may provide a general indication about numerical dispersion and diffusion properties of nonlinear schemes when applied to smooth solutions, it does not account for the concurrent presence of a wide range of scales in realistic flow fields. Hence, such effects as nonlinear interaction of modes and mode generation due to nonlinearities are disregarded. A more general nonlinear spectral analysis (NSA) was proposed by Fauconnier and Dick [15,16], whereby a prescribed energy spectrum is assumed for the numerical solution, with randomly selected phases. The empirical dispersion relation is then extracted for each initial field, and averaged over many realizations to achieve a statistically meaningful ensemble, thus allowing to characterize numerical dispersion and diffusion in wavenumber space. Comparison of the NSA results with EDR showed significant differences, and revealed that nonlinearity does affect the actual behavior of the mean modified wavenumber. A second essential property of numerical schemes is their cost/error balance. Although often disregarded, this property is of special importance in large-scale computations, in which one is constrained by the available computer time. A third property of obvious importance is the behavior of shock-capturing schemes at shocks. In this respect, it is well known that accuracy of any shock-capturing scheme degrades to first order downstream of shocks [17–19], mainly because locally $O(h)$ numerical viscosity must be injected to stabilize shock computations. Methods to remove first-order errors at shocks were discussed by Kreiss et al. [20], but these are difficult to apply to practical problems. Possible alternatives include the use of front tracking techniques, which by the way faces substantial problems in complex flows [21].

It is a commonly followed procedure to evaluate the properties of shock-capturing schemes on a case-by-case basis, and most frequently from visual comparison of numerical solutions, rather than quantitative data evaluation. In an attempt to achieve greater generality and possibly lay down a standardized basis for comparison, we herein present a unified framework, which includes existing tools for spectral analysis and cost/error balance evaluation, as well as a novel standardized procedure for evaluating numerical errors locally arising at shocks. The tools of analysis are presented in the forthcoming Section 2, and results of the evaluation of various schemes are presented in Section 3. Concluding remarks are given in Section 4.

2. Error analysis

In the present Section we identify suitable error metrics for the systematic characterization of shock-capturing schemes. In general terms, we stipulate that errors fall into two main categories: i) the propagation error associated with advection of disturbances, which is spatially distributed, and which accumulates in time; ii) the shock-capturing error, associated with nonlinear behavior of shock-capturing schemes at jumps, which is larger in magnitude, but concentrated in space. In the following, we briefly outline the analysis of the propagation error developed by Pirozzoli [14], which is also instrumental for the systematic evaluation of the computational efficiency, and then introduce a novel strategy for quantitative evaluation of the shock-capturing error.

2.1. Propagation error

We model the propagation error based on the scalar linear advection equation in a periodic domain, considering monochromatic sinusoidal initial conditions with wavelength λ and wavenumber $w = 2\pi/\lambda$,

$$\frac{\partial u}{\partial t} + c\frac{\partial u}{\partial x} = 0, \quad u(x,0) = \hat{u}_0 e^{iwx}, \tag{1}$$

where c is the advection speed. A semi-discrete approximation of Eq. (1) on a mesh with uniform spacing h and nodes $x_j = jh$, yields

$$\frac{dv_j}{dt} + cDv_j = 0, \tag{2}$$

where $v_j(t) \approx u\left(x_j, t\right)$, and D denotes a general (linear or nonlinear) space derivative approximation. In the case of linear approximations of the type

$$Dv_j = \frac{1}{h}\sum_{\ell=-p}^{q} a_\ell v_{j+\ell}, \tag{3}$$

a modified wavenumber is generally introduced to characterize the numerical dispersion and diffusion introduced by numerical discretization [22]

$$\Phi(\varphi) = \frac{1}{i}\sum_{\ell=-p}^{q} a_\ell e^{i\ell\varphi}, \tag{4}$$

where $\varphi = wh$ is the reduced wavenumber. Ideally, $\Phi \equiv \varphi$.

For nonlinear approximations of the space derivative operator one can nevertheless introduce an EDR [14] by advancing the solution up to a very short time (say τ), and Fourier transforming the numerical solution to obtain the numerical wave amplitude, corresponding to the reduced wavenumber φ, say $\hat{v}(\varphi;\tau)$ for all supported modes, thus obtaining

$$\Phi(\varphi) = -\frac{1}{i\sigma}\log\left(\frac{\hat{v}(\varphi;\tau)}{\hat{u}_0(\varphi)}\right), \tag{5}$$

where $\sigma = c\tau/h \ll 1$. Despite some limitations (discussed in the original reference), the resulting EDR accounts to leading order for the nonlinear effects embodied in shock-capturing schemes. Specifically, the dispersion error may be identified based on deviations of the real part of Φ from φ, and the diffusion error based on the imaginary part of Φ. Fuller control on the effect of nonlinearities, as well as account of the actual spectral content may be achieved through NSA [15,16], however EDR is retained in the present work for the sake of simplicity of implementation.

2.2. Computational efficiency

Based on the above given EDR, rigorous error metrics may be introduced for shock-capturing schemes. The analysis of broadband wave propagation of Colonius and Lele [2] and Pirozzoli [23] shows that, for disturbances with wavenumber range $0 \le w \le \bar{w}$ is

$$E(\bar{\varphi}) = \frac{1}{\bar{\varphi}}\max_{0\le\varphi\le\bar{\varphi}}\left|\Phi(\varphi) - \varphi\right|, \tag{6}$$

where $\bar{\varphi} = \bar{w}h$, hence it entirely depends on the EDR of the numerical scheme. In addition, assuming that time integration is performed by means of an explicit Runge–Kutta scheme at fixed Courant number $\sigma = ck/h$, the incurred computational cost is [2]

$$C \sim \frac{\mu}{\sigma\bar{\varphi}^{n_D+1}}, \tag{7}$$

where n_D is the number of spatial dimensions and μ is a (machine-dependent) measure of the scheme grind time, i.e. CPU time per grid point per time step. The EDR analysis given in the previous Section can thus be used to quantitatively characterize the computational efficiency of shock-schemes in terms of cost/error balance.

2.3. Shock-capturing error

In order to analyze the performance of finite-difference shock-capturing schemes we consider the scalar model problem introduced by Casper and Carpenter [17], consisting in the linear propagation of sinusoidal disturbances in a medium with abrupt change of the speed of sound. Specifically, Eq. (1) is considered with

$$c = \begin{cases} c_1, & x \le 0 \\ c_2, & x > 0 \end{cases}, \tag{8}$$

with $c_1 > c_2 > 0$. This inviscid model may be thought of as approximating the case of refraction of sound waves at the interface of solid media with different acoustic impedances. The characteristic lines enter the discontinuity standing at

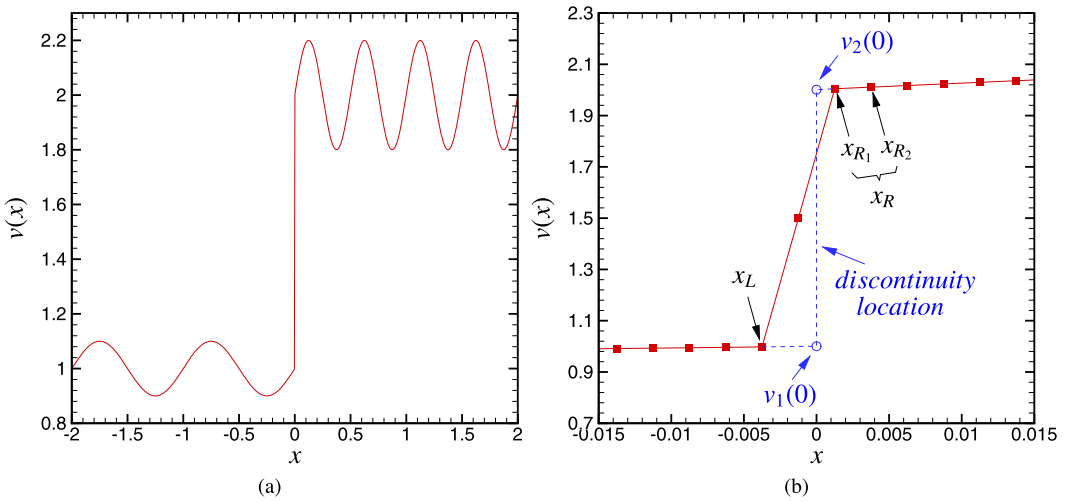

Fig. 1. Sound wave refraction test case, with $-2 \le x \le 2$, $w_1 = 2\pi$, $\epsilon = 0.1$, $c_1 = 2$, $c_2 = 1$; x_L and x_R are upstream and downstream monitoring points close to discontinuity which is fixed at $x = 0$. $v_1(0)$ and $v_2(0)$ are, respectively, the extrapolated left and right states of the numerical solution across the shock. (a) global view, (b) local view.

$x = 0$ from the left and exit from right, thus making this problem a convenient simplified testbed to analyze shock-sound interaction problems. Considering incoming sinusoidal disturbances of amplitude $\epsilon_1 = \epsilon$ and wavenumber w_1 upstream of the discontinuity, the following exact solution is found after an initial transient

$$u(x,t) = \begin{cases} u_1(x,t) = c_2 + \epsilon_1 e^{iw_1(x-c_1t)}, & x \le 0 \\ u_2(x,t) = c_1 + \epsilon_2 e^{iw_2(x-c_2t)}, & x > 0 \end{cases}, \tag{9}$$

where $\epsilon_2 = \epsilon c_1/c_2$, $w_2 = w_1 c_1/c_2$, and which satisfies the Rankine–Hugoniot jump relations

$$c_1 u_1(0,t) = c_2 u_2(0,t). \tag{10}$$

The numerical solution is monitored at two points (see Fig. 1), one just upstream of the shock (x_L) and one downstream of it (x_R, for which several choices will be considered), where the complex amplitudes of the numerical solution (say, $\hat{v}_1(x_L)$, $\hat{v}_2(x_R)$) are estimated by Fourier-transforming the solution in time at the forcing frequency $\omega = w_1 c_1$. Assuming that the wave propagation error is negligible in the vicinity of the discontinuity, the complex wave amplitudes are then extrapolated at the shock location according to

$$\hat{v}_1(0) = \hat{v}_1(x_L) e^{-iw_1 x_L}, \quad \hat{v}_2(0) = \hat{v}_2(x_R) e^{iw_2 x_R}, \tag{11}$$

which may be interpreted as 'left' and 'right' shock states (see Fig. 1(b)). This allows to define a numerical transfer function for disturbances crossing the discontinuity

$$\chi(w; \epsilon, c_1, c_2) = \frac{\hat{v}_2(0)}{\hat{v}_1(0)}. \tag{12}$$

For reference, the transfer function for the exact solution given in Eqn. (9) has $\tilde{\chi} = c_1/c_2$, i.e. there is no phase delay, and the variation of the amplitude of the disturbance is independent of the incident wavenumber. Expressing χ in terms of modulus and phase, $\chi = |\chi| e^{i\theta}$, we then define an amplitude error

$$\varepsilon_A = \frac{|\chi|}{|\tilde{\chi}|} - 1, \tag{13}$$

gauging the over/undershoot of the numerical solution downstream of the shock as a fraction of the exact amplitude, and a phase error

$$\varepsilon_P = \theta, \tag{14}$$

representing the concentrated phase shift of the numerical solution occurring at the jump. The total numerical error downstream of the shock can be likewise defined as

$$\varepsilon_T = \frac{\left|\hat{v}_2(0) - \tilde{\chi}\hat{v}_1(0)\right|}{\left|\tilde{\chi}\hat{v}_1(0)\right|} = \left|\frac{\chi}{\tilde{\chi}} - 1\right|. \tag{15}$$

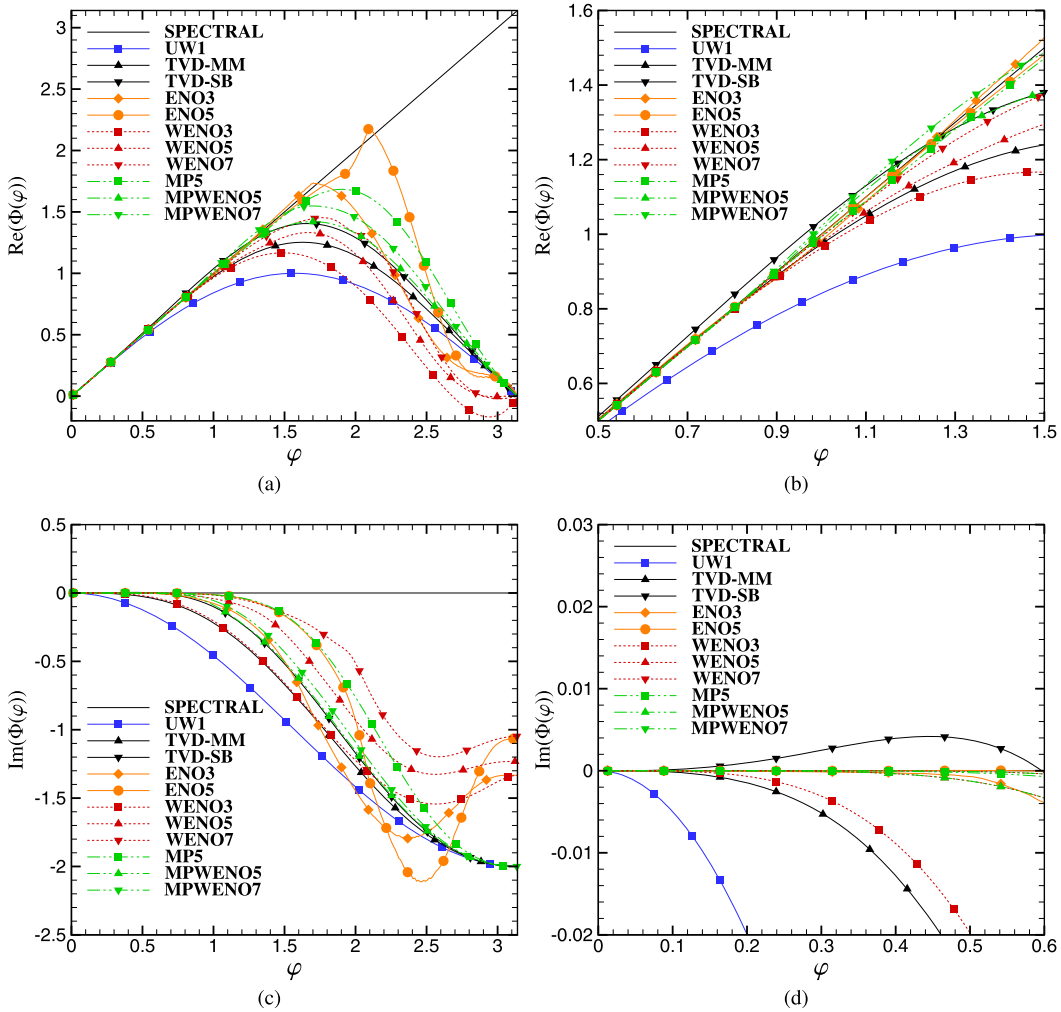

Fig. 2. Empirical dispersion relation for various shock-capturing schemes. The real (a, b) and the imaginary (c, d) parts of the modified wavenumber Φ are related to numerical phase speed and to numerical diffusion, respectively. (a, c): global view, (b, d): local view.

3. Performance of common shock-capturing schemes

For illustrative purposes, in this study we consider a limited number of representative shock-capturing schemes, including: (i) first order upwind scheme (UW1); (ii) second-order TVD schemes of the type developed by Osher and Chakravarthy [6], with minmod (MM) and superbee (SB) flux limiters; (iii) schemes of the ENO class [7], with formal order of accuracy of three (ENO3) and five (ENO5); (iv) schemes of the WENO class [8], with formal order of accuracy of three (WENO3), five (WENO5) and seven (WENO7); (v) the monotonicity-preserving scheme of Suresh and Huynh [9], with fifth-order accuracy (MP5); (vi) monotonicity-preserving weighted essentially non-oscillatory schemes of Balsara and Shu [10], with formal order of accuracy of five (MPWENO5), and seven (MPWENO7). For an extensive review of the properties of WENO and MPWENO schemes, and for a compilation of weights and smoothness indicators, the reader is referred to Balsara and Shu [10]. We point out that, although results are here shown only for a limited number of schemes, the following analysis may be applied to any other scheme.

3.1. Empirical dispersion relation

The EDR resulting from the analysis developed in Section 2.1 are shown in Fig. 2, in terms of real and imaginary part of the modified wavenumber Φ defined in Eq. (5), again recalling that they are respectively associated with numerical phase speed and with numerical diffusion. Consistent with expectations, the figure shows that TVD schemes, which have relatively low order of accuracy, tend to depart quickly from the ideal behavior, injecting substantial numerical diffusion also to well-resolved waves. Interestingly, the analysis also indicates that the TVD-SB scheme has slightly negative numerical diffusion at low wavenumbers, where $\mathrm{Im}(\Phi) > 0$. This feature is associated with the well known squaring effect caused by

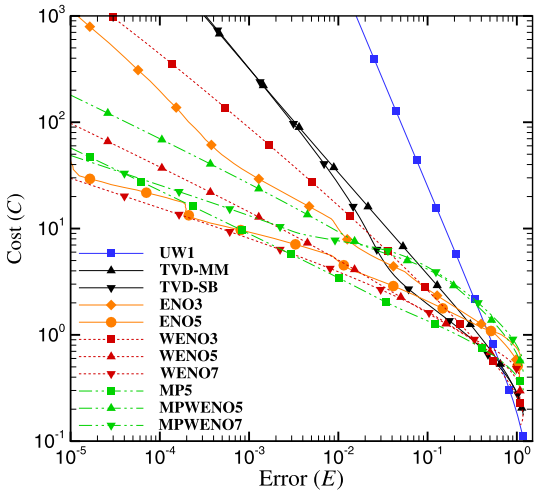

Fig. 3. Estimated computational cost (Eq. (7)) as a function of target relative error (Eq. (6)) in one space dimension ($n_D = 1$), for various shock-capturing schemes. The grind times used for the cost estimate are given in Table 1.

Table 1
Estimated CPU time per grid point per time step (grind time) for several shock-capturing schemes, normalized by the cost of the UW1 scheme.

UW1	TVD-MM	TVD-SB	ENO3	ENO5	WENO3	WENO5	WENO7	MP5	MPWENO5	MPWENO7
1	2.14	2.44	3.14	4.47	1.91	2.98	4.39	2.96	4.34	5.36

the superbee limiter, and which is compensated by the TVD nonlinear stability properties. ENO3 and ENO5 schemes exhibit good performance in terms of numerical dispersion, with strong numerical diffusion at high wavenumbers. For both of them the numerical phase speed exceeds the exact one up to $\varphi \approx 1.5$. WENO schemes have poorer dispersive properties, and for instance WENO3 propagates waves around $\varphi \approx \pi$ at negative phase speed, but they inject less numerical diffusion in the marginally revolved waves range. As expected, the behavior of WENO schemes strongly depends on the order of accuracy, and for instance the WENO3 scheme has a similar behavior as TVD schemes. The MP5 scheme is probably optimal among all the tested schemes in terms of both dispersion and diffusion properties, showing a very regular behavior. MPWENO schemes yield improved behavior in terms of dispersion over WENO schemes with same order of accuracy, but they also yield larger numerical diffusion. A weak overshoot over the reference value is also observed for these schemes in the numerical wave speed at intermediate wavenumbers.

3.2. Computational efficiency

The results of the efficiency analysis carried out in Section 2.2 are reported in Fig. 3. For that purpose, following Colonius and Lele [2], cost/error maps are considered, whereby for any given maximum reduced wavenumber to be resolved ($0 < \overline{\varphi} \leq \pi$), the required cost is estimated from Eqn. (7), and the incurred normalized error is estimated from Eqn. (6). Indicative computational cost figures have been obtained based on the measured CPU time for several one-dimensional computations, yielding the relative grind times reported in Table 1 to be used in Eqn. (7). In general terms, and as expected, all schemes exhibit increased computational cost for stricter error bounds, the scaling rate being dictated by the formal order of accuracy in the vanishing error limit. Despite their larger grind time, high-order schemes are found to require lower computational resources for given accuracy, as their performance in wavenumber space is better (recalling Fig. 2). This is especially true if greater accuracy is required, whereas classical second-order TVD schemes are competitive if relative errors of about 1% are allowed. ENO schemes are found to be marginally more efficient than WENO schemes, for given order of accuracy, despite the extensive use of logical instructions. The MP5 scheme seems to be the optimal one within schemes with the same formal order of accuracy. However, introduction of the MP bounds in WENO schemes yields poorer computational performance, especially at large values of the relative error. This analysis may be instrumental to predict the practical performance of a given numerical scheme, or to compare different schemes in wave propagation problems, but we should recall again that the assumption of smooth solutions is used.

3.3. Shock-capturing error

The shock-capturing error of the shock-capturing schemes presented so far has been evaluated according to the guidelines outlined in Section 2.3. Numerical simulations of the model sound wave refraction test case have been carried out in the space interval $-2 \leq x \leq 2$, with the following baseline conditions, $w_1 = 2\pi$, $\epsilon = 0.1$, $c_1 = 2$, $c_2 = 1$, with downstream

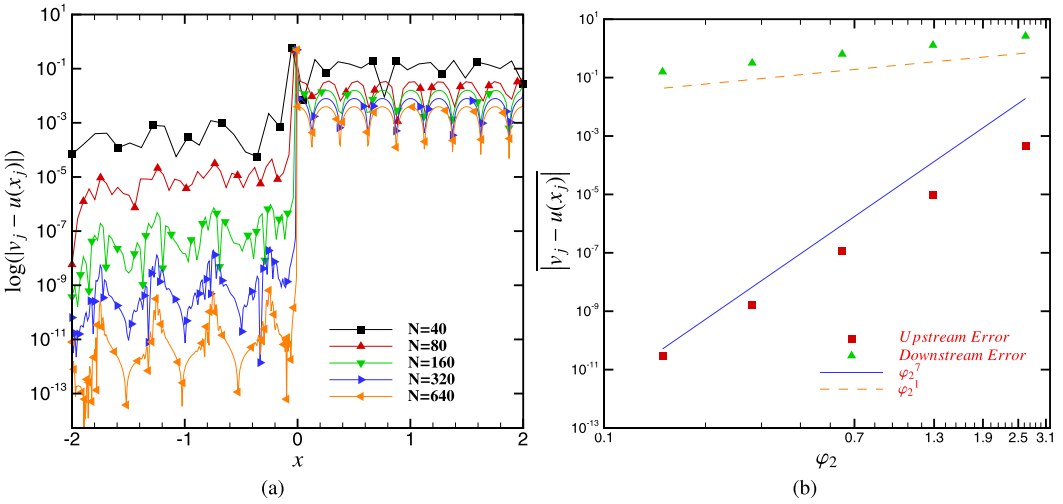

Fig. 4. Sound wave refraction test case with the baseline conditions ($w_1 = 2\pi$, $\epsilon = 0.1$, $c_1 = 2$, $c_2 = 1$, $-2 \le x \le 2$) using WENO7 scheme on a sequence of progressively refined meshes (N is the number of grid points). (a) distribution of pointwise error; (b) spatially averaged error, alongside with reference trends.

diagnostic point at x_{R_2} (see Fig. 1(b)). Several values of the mesh spacing have been considered to cover the range of reduced wavenumbers. Time integration is carried out by means of a third-order Runge–Kutta algorithm, at sufficiently low Courant number that the time stepping error is negligible. As well known [17], any shock-capturing scheme is first-order accurate downstream of shocks. This feature is clearly visible in Fig. 4, where we show the distribution of the local error for a numerical simulation carried out with the WENO7 scheme on a sequence of progressively refined meshes, and its spatial average on each side of the discontinuity. The expected h^7 decay of the local error is observed upstream of the shock, but barely first-order decay is recovered downstream of it. Nevertheless, we find that different shock-capturing schemes have qualitatively different behavior at shocks. For illustrative purposes, in Fig. 5 we show numerical results obtained with various schemes, compared with the analytical solution given in Eqn. (9). Corresponding to the selected number of points ($N = 50$), the reduced wavenumber upstream of the shock is $\varphi_1 = w_1 h \approx 0.5$, and downstream of it $\varphi_2 = w_2 h \approx 1$. Under these conditions significant wave propagation error is noticeable already upstream of the shock, where higher-order schemes clearly show less numerical diffusion. Downstream of the shock high-order schemes show clear phase delay, apparently introduced locally at the shock position, and attenuation associated with propagation error, which seems to be less for MP-limited schemes and high-order WENO schemes. Focusing on the near-shock region, it further appears that certain schemes, namely ENO5, WENO5, WENO7 even overshoot the analytical solution downstream of it, thus locally exhibiting anti-diffusive behavior. The general conclusion which can be drawn from the figure is that the overall performance of numerical schemes in shock/wave interactions is dictated by the concurrent effect of wave propagation and shock-capturing errors.

A spectral representation of the amplitude and phase errors for the various schemes is provided in Fig. 6, where ε_A, ε_P, ε_T defined in Eqns. (13), (14), (15) are depicted as a function of the reduced wavenumber past the shock. As also confirmed by log-log representation (not shown), we find the amplitude error to scale quadratically for small φ_2 for all the schemes here considered, except for TVD-SB and MP5, which only exhibit linear convergence. The phase error is found to increase linearly at small φ_2 for all schemes, hence it is dominant for well-resolved waves, and as a consequence the overall error downstream of the shock also scales linearly for $\varphi_2 \to 0$. Some unexpected behavior is observed in the spectral error distributions. Regarding the amplitude error, whereas most schemes have the expected behavior of low-pass filters and provide consistent damping mainly on the least resolved waves, some others are responsible for over-amplification of disturbances (associated with positive values of ε_A), in a more or less extended range of wavenumbers. Specifically, this occurs around $\varphi_2 \approx 0.4$ for TVD and MP schemes, whereas even higher over-amplification is observed around $\varphi_2 \approx 1$ for high-order ENO and WENO schemes. The use of MP limiters in WENO schemes has the effect of suppressing any numerical overshoot, yielding consistent numerical wave damping. Regarding the phase error, a lagging behavior (positive ε_P) is observed for all schemes for well-resolved waves, and phase lead is observed for marginally resolved ones, with MPWENO schemes showing the best performance, and the MP5 scheme delivering the poorest performance, after UW1. Finally, high-order ENO schemes tend to have a rather erratic behavior of the amplitude and phase errors. As previously pointed out, although all schemes are formally first-order accurate downstream of the shock, large differences exist in absolute terms. For well-resolved waves (say, $\varphi_2 \lesssim 0.8$) MPWENO schemes have much smaller error than other schemes, which makes them good candidates for shock capturing. MP limiters alone introduce large errors, whereas all other schemes are in between. For more marginally resolved waves the overall error increases for all schemes, however MPWENO schemes retain some limited advantage.

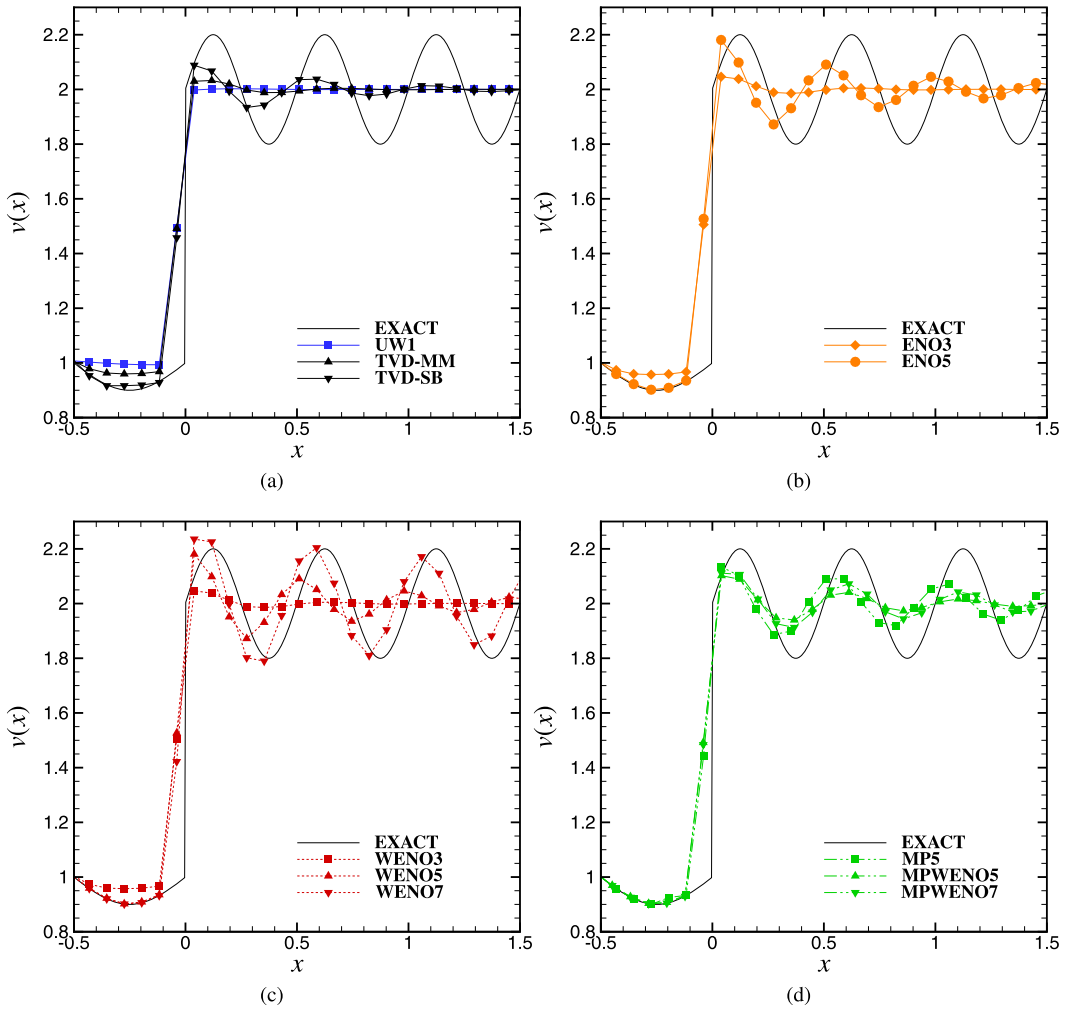

Fig. 5. Computed solutions for model sound wave refraction test case with the baseline conditions ($w_1 = 2\pi$, $\epsilon = 0.1$, $c_1 = 2$, $c_2 = 1$, $-2 \le x \le 2$), using $N = 50$ grid points (corresponding to $\varphi_2 \approx 1$), at $t = 8$.

In order to test the robustness of the shock-capturing error analysis carried out in this Section, in Fig. 7 we test the effect of changing several parameters for the model problem, namely the position of the monitoring point downstream of the shock, the ratio of the speed of sound across the shock, and the incoming wave amplitude. For illustrative purposes, only results obtained with WENO schemes are reported. Fig. 7(a–b) indicates that when the monitoring point is moved closer to the shock ($x_R = x_{R_1}$, see Fig. 1), the amplitude error slightly decreases because of reduced impact of the numerical propagation error. The effect on dispersion is even less evident, the main difference being stronger phase lead for $\varphi_2 > 1$. Increasing the speed of sound ratio (see Fig. 7(c–d)), larger errors are generally found, with stronger damping of waves from WENO3, and even higher overshoot for WENO7 around $\varphi_2 = 1$. The effect of increasing the amplitude of the incident wave to $\epsilon = 0.2$ (see Fig. 7(e–f)) is again to exacerbate errors for WENO5 and WENO7 schemes, thus bringing to light their strongly nonlinear behavior, whereas WENO3 has nearly linear response in this respect. In general, we find that the qualitative conclusions of the spectral shock error analysis will not change when the controlling parameters of the model problem are varied, which gives confidence for the generality of the results herein reported.

3.4. Numerical tests for 1D Euler equations

To verify the practical validity of the analysis carried out for the linear model equation, we have further considered a case of shock/entropy wave interaction which is a slight variation of the classical Shu–Osher test case. The one-dimensional Euler equations are solved in the interval $[-0.5, 10]$, with initial conditions

$$(\rho, u, p) = \begin{cases} (1 + 0.2\sin(5x),\ 3.54964,\ 1\ \ \ \ \ \ \ \ ), & x < 0 \\ (3.85714\ \ \ \ \ \ \ ,\ 0.92028,\ 10.33333), & x \ge 0 \end{cases}, \tag{16}$$

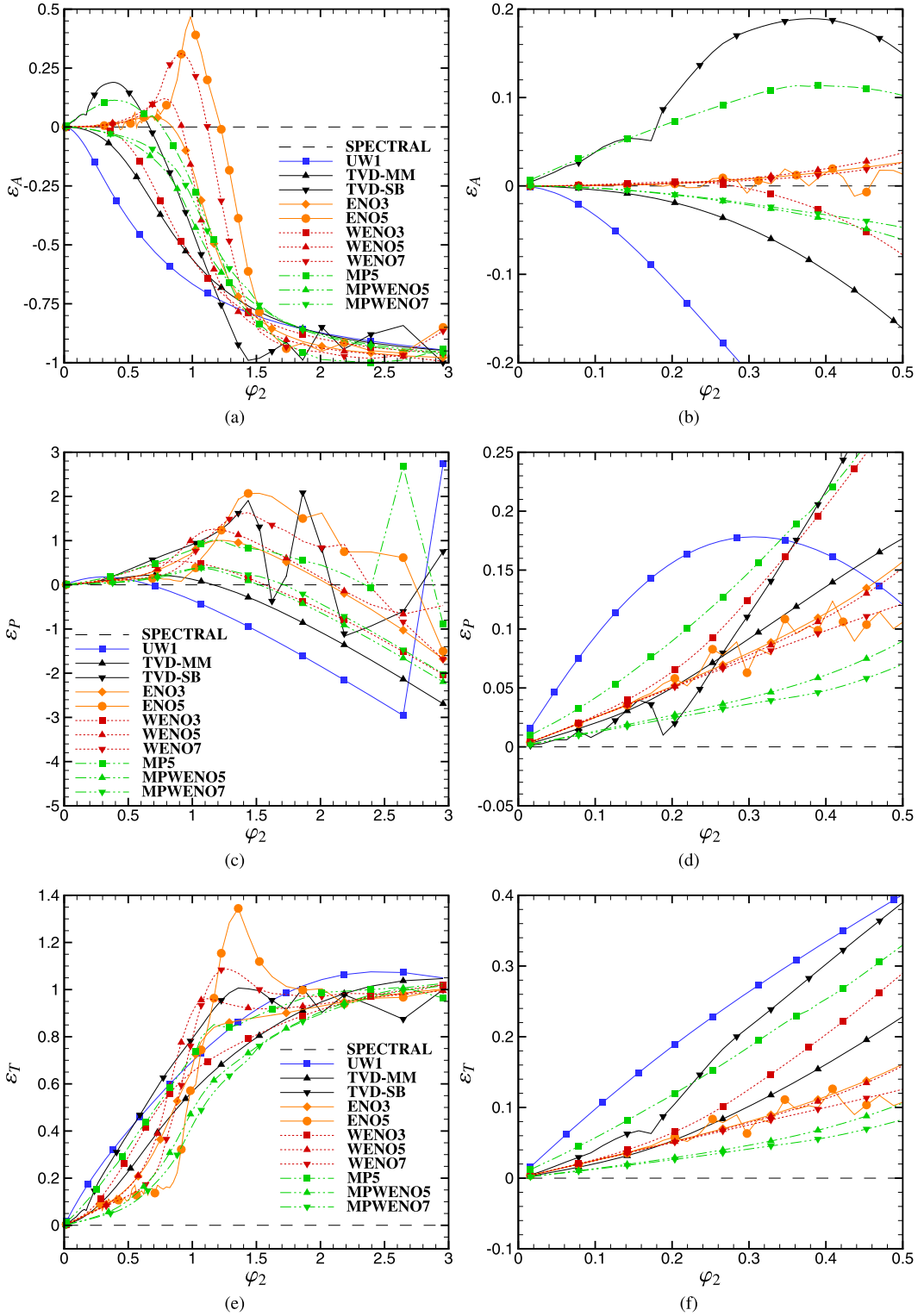

Fig. 6. Spectral distribution of shock-capturing error for model sound wave refraction test case, as a function of downstream reduced wavenumber, under the baseline condition ($w_1 = 2\pi$, $\epsilon = 0.1$, $c_1 = 2$, $c_2 = 1$, downstream monitoring point at x_{R_2}). (a, c, e): global view, (b, d, f): local view.

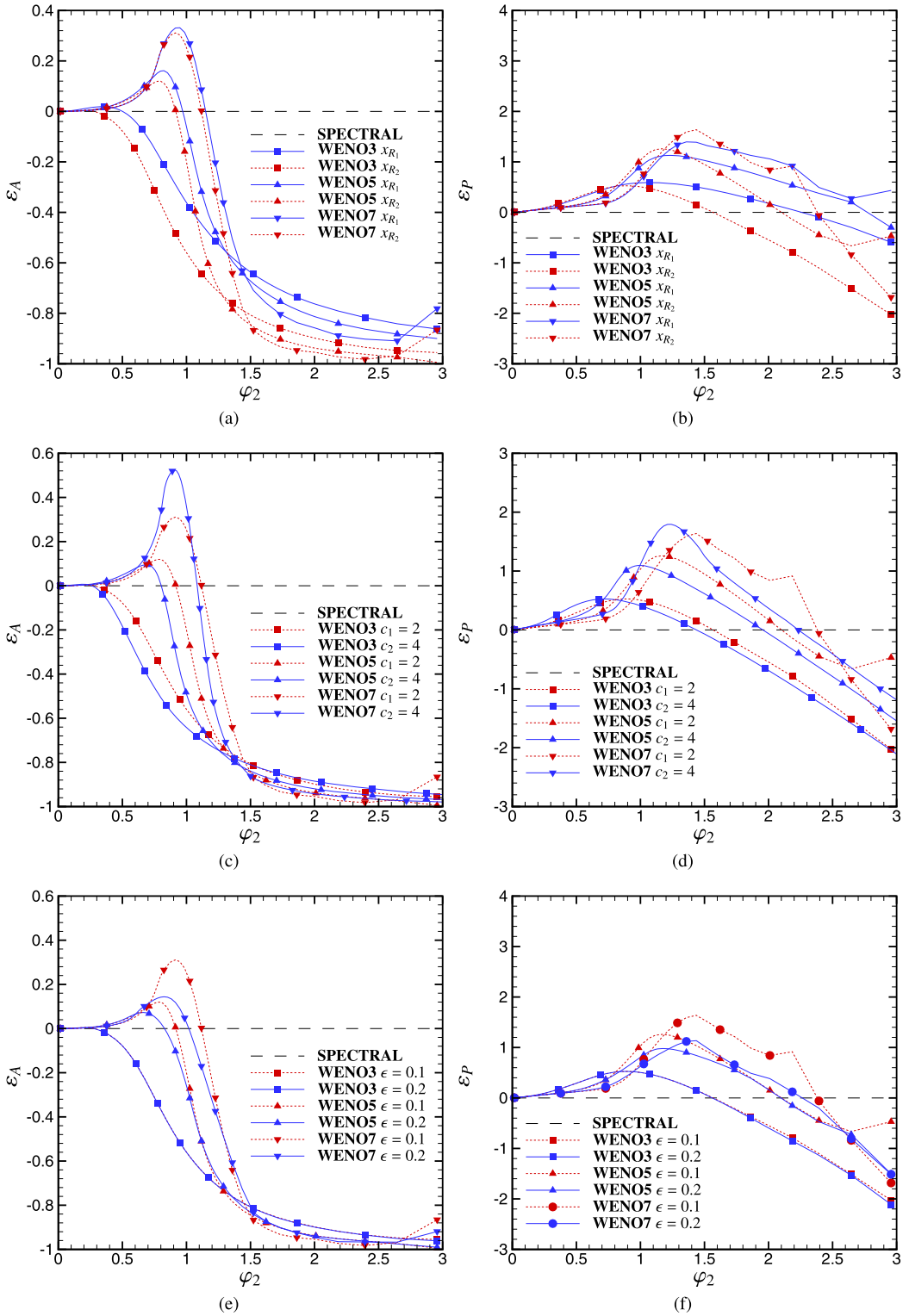

Fig. 7. Spectral distribution of shock-capturing error for model sound wave refraction test case, as a function of downstream reduced wavenumber, under the baseline condition ($w_1 = 2\pi$, $c_2 = 1$, $-2 \le x \le 2$). Effect of: position of downstream monitoring point (a-b), speed of sound ratio (c–d), and amplitude of incoming wave (e–f). (a, c, e): amplitude error, (b, d, f): phase error.

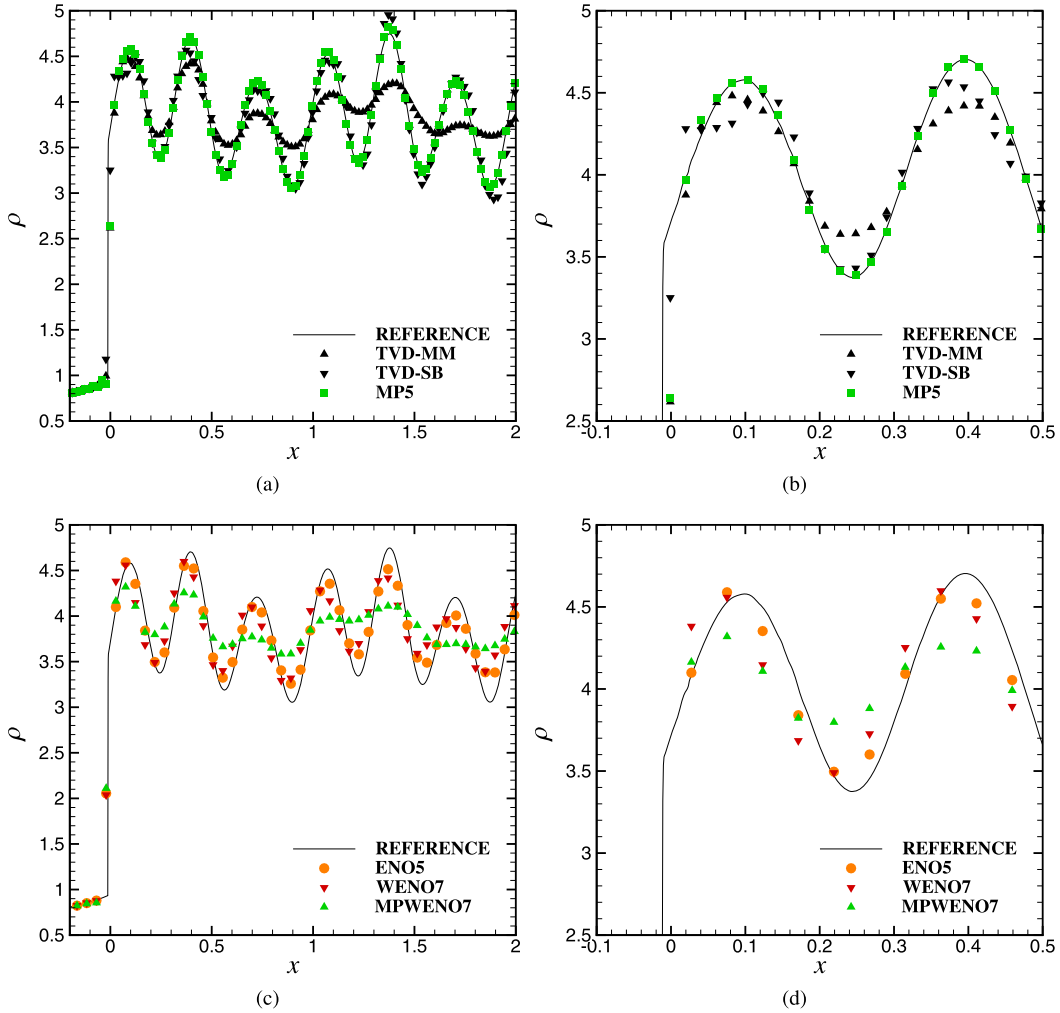

Fig. 8. Computed density distributions for one-dimensional shock/entropy wave interaction test case ((a, c), global view, (b, d), local view). Numerical solutions are obtained for downstream reduced wavenumber $\varphi_2 = 0.4$ (a, b), and $\varphi_2 = 0.925$ (c, d). The solid lines denote the reference numerical solution.

modeling the interaction of a sine density wave with a steady shock located at $x = 0$. All simulations are carried out at CFL number of 0.6, and the Steger–Warming flux splitting is used for upwinding. The simulations have been conducted over a sufficiently long time interval that any initial transient has been washed away. Since no exact solution exists for this problem, a reference numerical solution has been preliminarily fabricated with the WENO3 scheme using 12800 grid points. Fig. 8 shows the density distributions obtained with all shock-capturing schemes at time $t = 9.22$. To highlight specific features of each scheme, the mesh spacing has been selected in such a way to achieve desired values of the reduced wavenumber φ_2. All schemes maintain shock-capturing ability near the discontinuity, and show higher or lesser degree of numerical diffusion past the shock. Regarding the amplitude error, the figure confirms that TVD-SB and MP5 schemes exhibit a slight overshoot at the downstream monitoring point for $\varphi_2 = 0.4$ (see Fig. 6). However, a very different behavior is observed downstream of the shock, with the TVD-SB which has significantly less numerical diffusion than TVD-MM, however with tendency to overemphasize numerical extrema. As expected based on Fig. 6, the MP5 scheme also exhibits a slight overshoot at the monitoring point x_{R_2}, but it retains much better amplitude and phase accuracy downstream of the shock, thus supporting the conclusions of Suresh and Huynh [9]. The results of ENO and WENO schemes are shown in panels (c), (d) at coarse resolution ($\varphi_2 = 0.925$). Under these conditions, they exhibit significant density overshoots right past the shock, and significant phase shift with respect to the reference solution, which persists moving downstream. MPWENO schemes show more numerical damping than WENO schemes, thus supporting the conclusions of Balsara and Shu [10]. However, their phase error is less than other high-order schemes. In general, the observed trends are in good agreement and tend to support the validity of the conclusions reached in Section 3.3 based on the model linear problem.

4. Conclusion

We have introduced a standardized procedure for the quantitative evaluation of shock-capturing schemes, which includes analysis of the wave propagation performance through an empirically derived numerical dispersion relation (EDR), a cost/error balance analysis, and a novel spectral analysis of the shock-capturing error. This procedure is intended to go beyond the conventional approach of evaluating shock-capturing schemes on a case-by-case basis, and provides a useful platform for cross-scheme comparison. It is important to note that, given the inherent nonlinearity of the algorithms under scrutiny, it is impossible to characterize their behavior through any finite set of numerical experiments, as is the case here. Hence, although we believe that the results of the analysis herein developed are representative of the actual behavior of numerical schemes, they do not necessarily apply to all possible test cases.

The baseline EDR has been used to characterize the numerical dispersion and diffusion errors of common schemes. Although more sophisticated approaches are possible [15] which better account for nonlinear effects and spectral distribution of energy across wavenumber space, we find that EDR well highlights certain features which are not evident from linear analyses, as for instance the weakly unstable behavior of TVD schemes incorporating the superbee limiter. High-order ENO and WENO schemes are found to have similar behavior, with better dispersive properties for ENO, and less numerical diffusion for WENO. A good compromise as far as wave propagation properties is concerned is found to be the MP5 scheme [9]. Regarding the computational efficiency, we confirm that high-order schemes have generally better cost/error balance, especially when strict admissible error bounds are placed. ENO schemes are found to be slightly more efficient than WENO schemes with the same order of accuracy. Further, the MP5 scheme is found to be slightly more efficient than all other fifth-order accurate schemes. Application of MP limiters to WENO schemes (MPWENO) implies additional computational cost, with no significant error reduction.

With regard to the shock-capturing error analysis, we do confirm that all shock-capturing schemes are first-order accurate downstream of shocks, however with important differences among them. The phase error is found to be dominant over the amplitude error, and in this respect shock-capturing schemes typically yield a lagging behavior. Analysis of the amplitude error shows that the amplitude of disturbances transmitted through shocks is generally underestimated. Notable exceptions to this common behavior include the TVD and the MP5 schemes, which are especially inaccurate in the range of well-resolved waves (i.e. low φ_2), and yielding over-amplification of waves around $\varphi_2 \approx 0.4$. A similar behavior is also observed for high-order ENO and WENO schemes, which yield exaggerated amplitude of transmitted waves for $\varphi_2 \approx 1$. This behavior is probably to be traced to the near-shock activation of linearly unstable stencils, both in ENO and WENO. Augmenting WENO schemes with MP limiters appears to be an effective strategy for shock-capturing, and MPWENO schemes yield the lowest overall numerical error among the tested schemes, and suppression of overshoots. Illustrative calculations have been carried out for the 1D Euler equations, which generally support validity of the analysis. The main benefit of the present analysis is the availability of precise metrics to rank shock-capturing schemes which, with all caveats stated above, may be also used for the synthesis of new schemes.

Acknowledgements

This work is supported by National Natural Science Foundation of China under Grants No. 11522222 and No. 11472305, Innovative Sustentation Fund for Excellent Ph.D. Students in Hunan province (No. CX2016B003), and Chinese Scholarship Council (CSC) (No. 201703170277) during a visit of Guoyan Zhao in Rome.

References

[1] Z. Wang, High-order methods for the Euler and Navier–Stokes equations on unstructured grids, Prog. Aerosp. Sci. 43 (2007) 1–41.
[2] T. Colonius, S.K. Lele, Computational aeroacoustics: progress on nonlinear problems of sound generation, Prog. Aerosp. Sci. 40 (2004) 345–416.
[3] S. Pirozzoli, Conservative hybrid compact-WENO schemes for shock–turbulence interaction, J. Comput. Phys. 178 (2002) 81–117.
[4] J. Von Neumann, R.D. Richtmyer, A method for the numerical calculation of hydrodynamic shocks, J. Appl. Phys. 21 (1950) 232–237.
[5] A.E. Mattsson, W.J. Rider, Artificial viscosity: back to the basics, Int. J. Numer. Methods Fluids 77 (2015) 400–417.
[6] S. Osher, S. Chakravarthy, High resolution schemes and the entropy condition, SIAM J. Numer. Anal. 21 (1984) 955–984.
[7] A. Harten, B. Engquist, S. Osher, S.R. Chakravarthy, Uniformly high order accurate essentially non-oscillatory schemes, III, in: Upwind and High-Resolution Schemes, Springer, 1987, pp. 218–290.
[8] G.-S. Jiang, C.-W. Shu, Efficient implementation of weighted ENO schemes, J. Comput. Phys. 126 (1996) 202–228.
[9] A. Suresh, H. Huynh, Accurate monotonicity-preserving schemes with Runge–Kutta time stepping, J. Comput. Phys. 136 (1997) 83–99.
[10] D.S. Balsara, C.-W. Shu, Monotonicity preserving weighted essentially non-oscillatory schemes with increasingly high order of accuracy, J. Comput. Phys. 160 (2000) 405–452.
[11] N.A. Adams, K. Shariff, A high-resolution hybrid compact-ENO scheme for shock–turbulence interaction problems, J. Comput. Phys. 127 (1996) 27–51.
[12] V.G. Weirs, G.V. Candler, Optimization of Weighted ENO Schemes for DNS of Compressible Turbulence, AIAA paper 97-1940, AIAA, 1997.
[13] M.P. Martín, E.M. Taylor, M. Wu, V.G. Weirs, A bandwidth-optimized WENO scheme for the effective direct numerical simulation of compressible turbulence, J. Comput. Phys. 220 (2006) 270–289.
[14] S. Pirozzoli, On the spectral properties of shock-capturing schemes, J. Comput. Phys. 219 (2006) 489–497.
[15] D. Fauconnier, E. Dick, On the spectral and conservation properties of nonlinear discretization operators, J. Comput. Phys. 230 (2011) 4488–4518.
[16] D. Fauconnier, E. Dick, Spectral analysis of nonlinear finite difference discretizations, J. Comput. Appl. Math. 246 (2013) 113–121.
[17] J. Casper, M.H. Carpenter, Computational considerations for the simulation of shock-induced sound, SIAM J. Sci. Comput. 19 (1998) 813–828.
[18] B. Engquist, B. Sjögreen, The convergence rate of finite difference schemes in the presence of shocks, SIAM J. Numer. Anal. 35 (1998) 2464–2485.
[19] M. Arora, P.L. Roe, On postshock oscillations due to shock capturing schemes in unsteady flows, J. Comput. Phys. 130 (1997) 25–40.

[20] G. Kreiss, G. Efraimsson, J. Nordström, Elimination of first order errors in shock calculations, SIAM J. Numer. Anal. 38 (2001) 1986–1998.
[21] A.K. Henrick, T.D. Aslam, J.M. Powers, Simulations of pulsating one-dimensional detonations with true fifth order accuracy, J. Comput. Phys. 213 (2006) 311–329.
[22] R. Vichnevetsky, J.B. Bowles, Fourier Analysis of Numerical Approximations of Hyperbolic Equations, vol. 5, SIAM, 1982.
[23] S. Pirozzoli, Performance analysis and optimization of finite-difference schemes for wave propagation problems, J. Comput. Phys. 222 (2007) 809–831.